Spectrochimica Acta Part A: Molecular and Biomolecular Spectroscopy 272 (2022) 120980

Contents lists available at ScienceDirect

Spectrochimica Acta Part A: Molecular and Biomolecular Spectroscopy

journal homepage: www.elsevier.com/locate/saa

Impact of silver nanoparticles size on SERS for detection and identification of filamentous fungi

Javier Christian Ramirez-Perez [a,*], Tatiana A. Reis [b], Cristiano L.P. Olivera [c], Marcia A. Rizzutto [a]

[a] Institute of Physics, Laboratory of Archaeometry and Science Applied to Cultural Heritage, University of Sao Paulo, Sao Paulo, Brazil
[b] Institute of Biosciences, Laboratory of Mycology of University of Sao Paulo, Sao Paulo, Brazil
[c] Institute of Physics, Complex Fluids Group of University of Sao Paulo, Sao Paulo, Brazil

HIGHLIGHTS

- AgNPs with sizes of 10, 30, and 60 nm were synthesized using wet-chemical reduction.
- The yield, shape, size, and homogeneity of AgNPs were evaluated using SAXS.
- The SERS intensity increases as the size of AgNPs increases from 10 to 60 nm.
- The SERS enhancement reached a maximum of $2.4x10^{5.}$
- SERS reproducibility was less than 20% for the four fungal strains studied.

GRAPHICAL ABSTRACT

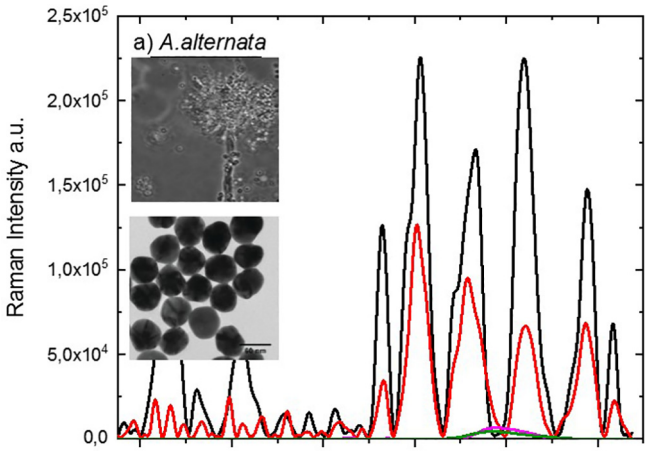

ARTICLE INFO

Article history:
Received 24 September 2021
Received in revised form 22 January 2022
Accepted 29 January 2022
Available online 4 February 2022

Keywords:
Biodeterioration
Biodegradation
Raman
SERS
Filamentous fungi
Silver nanoparticles
Detection
Identification

ABSTRACT

Using the proper size of nanoparticles as an active substrate, Surface-enhanced Raman scattering (SERS) can provide a reliable technique for detecting and identifying fungi, including *Alternaria alternata, Aspergillus flavus, Fusarium verticilliodes,* and *Aspergillus parasiticus* that have been associated to biodeterioration and biodegradation of cultural heritage materials. In this research spherical silver nanoparticles (AgNPs) of average size of 10, 30 and 60 nm were synthesized using the wet chemical method with good yield and their size and shape distributions were examined using small-angle X-ray scattering (SAXS). The protocol for fungi sample preparation proved to be critical for producing high-quality and reproducible SERS spectra. We found that the effect of AgNPs on SERS signal enhancement is size dependent under the same experimental conditions; the SERS intensity of fungal strains using 60 nm achieved up to $2.3x10^5$ enhancement, about twice as intense as those produced with 30 nm, and 10 nm produced a minor broad weak peak barely discernible around 1400 cm^{-1}, similar to the NR spectra profile in the 550–1700 cm^{-1} spectral region, and the SERS signals using 60 nm showed high reproducibility, with less than 20% variance. Furthermore, we used principal component analysis (PCA) to statistically classify the SERS spectrum into four separate clusters with 99 percent variability so that the four fungal strains could be clearly detected and identified. The SERS technique, in combination with the PCA developed in this

* Institute of Physics, University of Sao Paulo, Rua do Matào 1371, Sao Paulo,05508-090, Brazil
E-mail address: jperez@if.usp.br (J.C. Ramirez-Perez).

https://doi.org/10.1016/j.saa.2022.120980
1386-1425/

study, provides a simple, rapid, accurate, and cost-effective analytical tool for detecting and identifying filamentous fungal strains.

1. Introduction

Filamentous fungi are widespread environmental microorganisms. They are used to make pharmaceuticals, enzymes, organic acids and food, and some of them can become pathogenic and cause diseases like mycoses, which affect humans and other animals due to their tendency for producing mycotoxins [1–3]. Only a few strains are common pathogens, accounting for the majority of human infections as well as morbidity and mortality in immunocompromised peoples [3–5]. The majority of filamentous fungi strains are known to cause harm to organic materials used in cultural heritage objects, including cellulose fibers, paper-based books, documents, canvases, clothing, textiles, ceramic, leather, straw, natural hair or feathers, oil, casein, glue, and others [6,7]. These materials are suitable for filamentous fungi at various stages of development, including germination, hyphae, conidia, and mycelia, and they have a remarkable ability to grow in low temperatures and humidity [7,8]. Fungal spores can survive for a long time in these circumstances [9–11]. Fungal colonization of support materials (natural binders, oil seeds, casein, starch, etc.) is common because they excrete a battery of extracellular hydrolytic enzymes such as cellulases, pectinases, pectolytic enzymes, chitinases, glycosyl hydrolases, and proteases, which digest organic matter and alter and weaken those materials through enzymatic activities. [2,9,12]. Molds produce colored compounds that stain and discolor textiles, whereas fungi penetrate paint layers and migrate beneath them, resulting in paint layer disintegration, exfoliation, and detachment, as well as paint layer loss. Cellulases are excreted by fungi in paper, and cellulose degraders can cause substantial biodeterioration and biodegradation, affecting collections in museums, archives, and libraries around the world [5,9,13,14]. Some fungal strains hydrolyze long chain polymers to change their structure and use the resultant products as carbon and energy sources during biodegradation [10,11]. Traditional fungal identification relied on morphological characteristics, particularly those of reproductive structures. However, there are significant drawbacks to this method of identification, such as sterility of fungal cultures that have not established reproductive structures or morphological similarities between individuals of different strains [9,13]. Incorporation of molecular techniques into fungal taxonomy such as DNA/RNA extraction procedures, polymerase chain reaction (PCR) amplification, DNA-denaturing gradient gel electrophoresis (DGGE) has helped to solve such problems, at least in certain situations [13–15]. These methods, however, are not bias-free, and each step might have an impact on the final results. They contain problems as well, like polymerase mistakes, size limitations and/or non-specific priming and profiles parameter settings of bioinformatic analysis. Differences in DNA extraction methods, sequencing technology and platform usage result in data sets with nothing in common for a statistical comparison [16,17]. As a result, only a small number of taxa have sequence data accessible. Furthermore, molecular techniques are frequently costly, labor-intensive, time-consuming, and damaging, needing significant sample preparation and analysis by highly trained and experienced personnel. Minimum sample preparation, direct sample analyses, rapid automation, and low cost would be suitable methods for replacing these labor-intensive operations. Spectroscopic techniques provide a variety of qualitative and quantitative information about a particular sample, thanks to recent advances in analytical instrumentation. Normal Raman (NR) spectroscopy is a type of spectroscopy that uses molecular vibrational transitions to study biological systems [17,18]. Due to its intrinsic weak intensity in biological systems, where many of the target biomolecules are present at low concentrations, NR spectroscopy is relatively unselective with respect to the different compounds present in the biological milleu. Furthermore, in NR, there is typically a strong fluorescence background (intrinsic or impurity-derived), which degrades the spectral quality and reduces the signal-to-noise ratio [18]. Surface-enhanced Raman spectroscopy (SERS) is a contemporary spectroscopic technique in which the Raman signal of a Raman-active molecule's functional group is considerably enhanced when the molecule is adsorbed on the surface of specially noble metals like Ag and Au nanoparticles (NPs). In addition, the ability of SERS-active substrates to quench fluorescence improves the signal to noise ratio. Because of the substantial enhancement it gives with visible excitation wavelengths, AgNPs are the most commonly utilized metal, and aggregates are the preferred substrates for analytical applications, each compound's SERS spectrum is known to have a distinct "fingerprint." [1,19,20]. When light strikes metallic NPs, they generate extremely high local electric fields known as surface plasmon resonance (SPR), which provide an enhancement up to several orders of magnitude (10^{14}) higher than NR scattering [21,22]. So far, it was commonly accepted that two enhancing processes, one long-range electromagnetic (EM) effect and the other short-range chemical (CHEM) effect, were both active at the same time [21]. This can be attributed to the highly localized field of SPR, as well as the amplification of the electric field of both incident and scattered electromagnetic radiation, in resonance with adsorption on metal NPs. The chemical effect and the classical near-field electromagnetic effect are both responsible for SERS enhancement [23]. Changing the dimensions of nanostructures, their size, shape, spacing, and orientation, as well as the dielectric medium around them on which the molecules are adsorbed, can change the electric field intensity [23–26]. As a result, the ability of SERS-based metallic NPs to detect and identify a wide range of microorganisms, including filamentous fungus, is largely dependent on the size and shape of the NPs on which the biomolecules are adsorbed, in order to obtain high and reproducible SERS signals. A thorough NPs and fungi sample preparation protocol must be preceded before the sample is subjected to SERS measurement (Fig. 1).. Because the application of SERS to microorganisms is hindered by low signal reproducibility due to non-uniform distribution of NPs and analytes on the substrate surface, some investigations have coupled Raman with chemometric approaches to provide quantitative analysis and reproducible detection. Using the SERS technique, we investigate how the size of AgNPs impacts the detection and identification of filamentous fungi from four different strains: *Aspergillus flavus, Aspergillus parasiticus*; *Fusarium verticilliodes* and *Alternaria alternata*. Develop an experimental protocol that includes filamentous fungi cultivation, sample preparation for SERS analysis, and the synthesis and characterization of three AgNP sizes; validate the SERS technique for accuracy and reproducibility; demonstrate the significant SERS spectrum features and extract biochemical information generated among different fungi strains; and, finally, perform their identification using principal component analysis (PCA). .

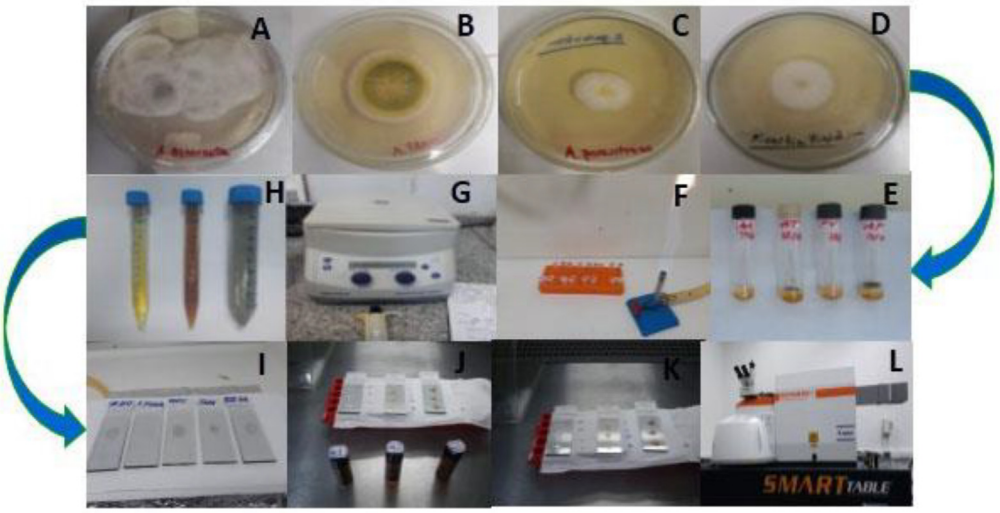

Fig. 1. Description of the experimental protocol: strains of fungal cultivation in NA, A) *A. alternata*; B) *A.flavus*; C) *A.parasiticus*; D) *F. verticilliodes*; E) cultivation in NB; F) Extraction with deionized water; G) Sample vortexed, washed and centrifugation; H) AgNPs of various sizes synthesized; I) Control samples; J) Clean fungal cells are mixed with AgNPs of various sizes and dropped on a CaF_2 glass slide.; K) Fungi-AgNPs SERS active substrate cast as dried thin film; L) Raman spectroscopy analysis: 1% (500 mW) 785 nm excitation, 10 s exposure time.

2. Materials and methods

2.1. Preparation of the fungal samples for SERS measurements

Four strains of different fungal strains namely: *A. flavus* (ATCC 204304), *F. verticilliodes* (ATCC 1442), *A. alternata* (ATCC 8739), and *A. parasiticus* (IMI 24264544) were included in the research. The strains, housed by the Department of Microbiology, Institute of Biomedical Sciences, Laboratory of Mycology, University of Sao Paulo, Brazil. First of all fungi strains were cultured in nutrient agar (NA), potato dextrose agar (PDA; Merck KGaA, Germany) and then cultivated in nutrient broth (NB), yeast extract sucrose broth (YES, Merck KGaA, Germany).

The experiments described here involved pure cultures of four fungi strains were stored at – 80 °C stocked, dissolved and inoculated in sterile slant test tubes (100 mL) containing PDA and incubated at 25 °C for 5 to 7 days in the dark, and after that held for 4–5 weeks at 4 °C. The filamentous fungi selected were cultured in 90 mm diameter Petri dished containing PDA, each plate was incubated at 25 °C for 5 days in the dark. A homogenous sample (conidia and hyphae) from a colony was collected by scraping with a sterile scalpel and suspending in 500 μL distilled water (DI) in a 1.5 mL microtube, avoiding contamination by nutrients from culture media. The suspension was vortexed, rinsed, and centrifuged (12000 rpm/5 min); following centrifugation, the pellet was washed and re-suspended in a new 500 μL DI water, and the process was repeated three times. The suspension (10 μL) was then transferred to a 2 mL glass tube containing NB, Yeast extract sucrose (YES) and incubated in the dark for 5 days at 25 °C, using a sterile plastic loop, a sample of fungi growing on the surface of the NB was taken from the broth and suspended in 500 μL DI water of 1 mL eppendorf tube. After vortexed and washed three times by centrifugation at 12000 rpm for 5 min, clean cells of fungi were suspended and kept in a 100 in μL eppendorf tube at 4 °C. In this method, the sample, extraction, collection and preparation of clean fungal cells in form of aqueous solution from the NB was straightforward and quick. Each strain studied had an average fungal concentration of 1.0×10^5 cfu/mL. For SERS testing a 5 μL aliquot of AgNPs of different sizes was spotted onto a CaF_2 glass slide, followed by a 5 μL solution of clean fungal cells deposited onto each substrate, and the mixture was homogenized with a 10 μL pipette. to serve as control, a 5 μL of clean fungal cells was spotted in the same CaF_2 glass slide. After forming a dried thin film, the samples were dried for about 10 min at room temperature before NR and SERS analysis. The experimental approach for the four fungi strains investigated is depicted in Fig. 1.

2.2. Preparation of silver nanoparticles

Wet chemical method was used to synthesize silver nanoparticles (AgNP) with glucose as a reducing agent and poly(N-vinylpyrrolidone) (PVP) as a capping agent. [23,28]. The method is described elsewhere [24]. Briefly, in 320 mL, 16 g of glucose and 8 g PVP were dissolved in water and heated to 90 °C. Then immediately dissolve 4 g $AgNO_3$ in 8 mL of the mixture. The temperature of dispersion was maintained at 90 °C. At different intervals during the process, aliquots were collected and chilled to room temperature. Fig. 1S (SM) displays the 3 aliquots collected under reaction times of 10 min (10 nm), 30 min (30 nm) and 120 min (60 nm) minutes, respectively. Our research group recently published a comprehensive structural characterization of AgNPs using the theoretical Small-angle X-ray scattering (SAXS) model, which assumes a system of polydisperse spheres, which is a good approximation for the shape of the formed nanoparticles as confirmed by transmission electron microscopy (TEM) images. [25], To obtain the particle size distribution of spheres that provided the best fit of the experimental data, The main equation of the Monte Carlo (MC) model is:

$$\mathbf{3.}\ :\boldsymbol{I}(\boldsymbol{q}) = \boldsymbol{Sc}\left\{\int_0^\infty \boldsymbol{V^2}(\boldsymbol{R})\boldsymbol{D}(\boldsymbol{R},\sigma)\boldsymbol{P_{sph}}(\boldsymbol{q},\boldsymbol{R})\boldsymbol{dR}\right\}\boldsymbol{S_G}(\boldsymbol{q},\boldsymbol{RG}) + \boldsymbol{B}$$

where: R is sphere radius, σ is the standard deviation of the radius distribution (polydispersity), Sc is the scale factor, V(R) is the sphere volume, D(R,σ) is the radius distribution function (Schulz Zimm), P_{sph} (q, R) is the sphere form factor, q scattering vector of the reciprocal space, S_G (q,RG) is the Guinier structure factor, RG is the gyration radius of aggregates and B is the background. The Guinier factor describes the scattering of clusters with gyration radius equal to RG [26]. Fig. 2 (SM) shows SAXS intensity curves and the radius distributions determined for each aliquot.

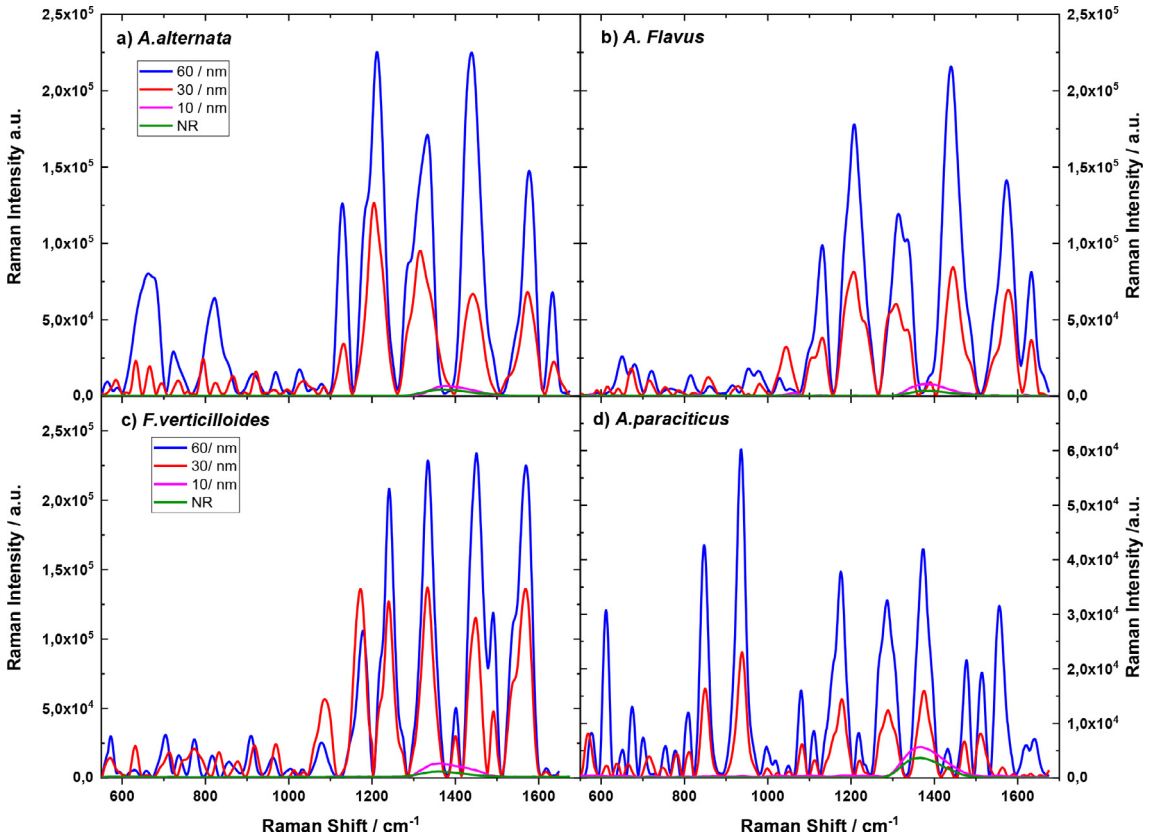

Fig. 2. Impact of AgNPs size (10, 30 and 60 nm) on SERS of: a) *A.alternata*, b) *A. flavus*, c) *F. verticilloides*, d) *A. parasiticus*. All spectra have been rubber baseline correction and shifted horizontally for improved visualization.

Table 1
Average diameter Φ (nm) of Silver nanoparticles.

Sample	Φ (nm)
$AgNP_1$	10.4 +/- 2.0
$AgNP_2$	30.4 +/- 3.3
$AgNP_3$	58.8 +/- 7.0

Table 1 shows average radius and polydispersity determined for each sample.

3.1. Raman spectroscopy

The SERS measurements were performed using a Renishaw Raman microscope inVia Reflex Raman Microscopy System Leica DM2500 M (Ranishaw PlC., New Mills, Wotton-under-Edge Gloucestershire, UK) equipped with 500 mW (maximum high power) diode laser emitting a 785 nm line which was used as an excitation source. The laser light was passed through a line filter and focused on a sample mounted on a tridimensional stage with 50x objective lens (numerical aperture 0.75) that focused the laser to a spot size around 2.5 um. The Raman scattering signals were recorded by using a 1040x256 pixel RenCam CCD array detector with thermoelectrically cooling, 1200 lines network of diffraction was employed. The instrument was calibrated using a silicon wafer with the band center at 520 cm^{-1}. During the measurement, just 1% of the nominal maximum high power light from the 785 nm diode laser was employed focused onto the sample at a microscope stage through a 50x objective with 10 s exposure time, and 10 accumulations.

3.2. Data processing

The OriginPro 2018.64 bit software was used to treat the NR and SERS spectra in this investigation. The AgNPs SERS active substrate was calibrated using pMBA typically standard SERS analyte, because it tends to adsorb efficiently on AgNPs surface [27]. The SERS active-substrate exhibits high sensitivity, an enhancement factor approximately $4.4x10^7$, reproducibility (RSD = 4%) and stability of near 2 months of the recorded SERS spectra Fig. 3S and 4S (SM). The detection and identification samples of four filamentous fungi strains namely *A. Alternata*, *A. flavus*, *F. verticilloides*, and *A. parasiticus* on three different substrates AgNPs of different sizes (10, 30 and 60 nm) onto CaF_2 glass slide samples were prepared by applying the same experimental protocol (Fig. 1). The NR and SERS spectra were tested 12 times on different spots within the same sample for each filamentous fungi and AgNPs substrate studied. The experiments were repeated three times over the course of the experimental investigation, which took place between April 30, June 05, August 06, and December 15, 2020.

4. Results and discussions

4.1. Impact of AgNPs sizes on the SERS method for detection and identification of fungi

The impact of AgNPs size on the SERS method for detecting and identifying four fungal strains including *A. Alternata, A. flavus, F. verticilloides, and A. parasiticus* was identical. Fig. 2 shows that the SERS intensity incrases with the size of silver nanoparticles from 30 and 60 nm, with the exception of silver nanoparticles of 10 nm, produce over a detection wavenumber range of 550 to

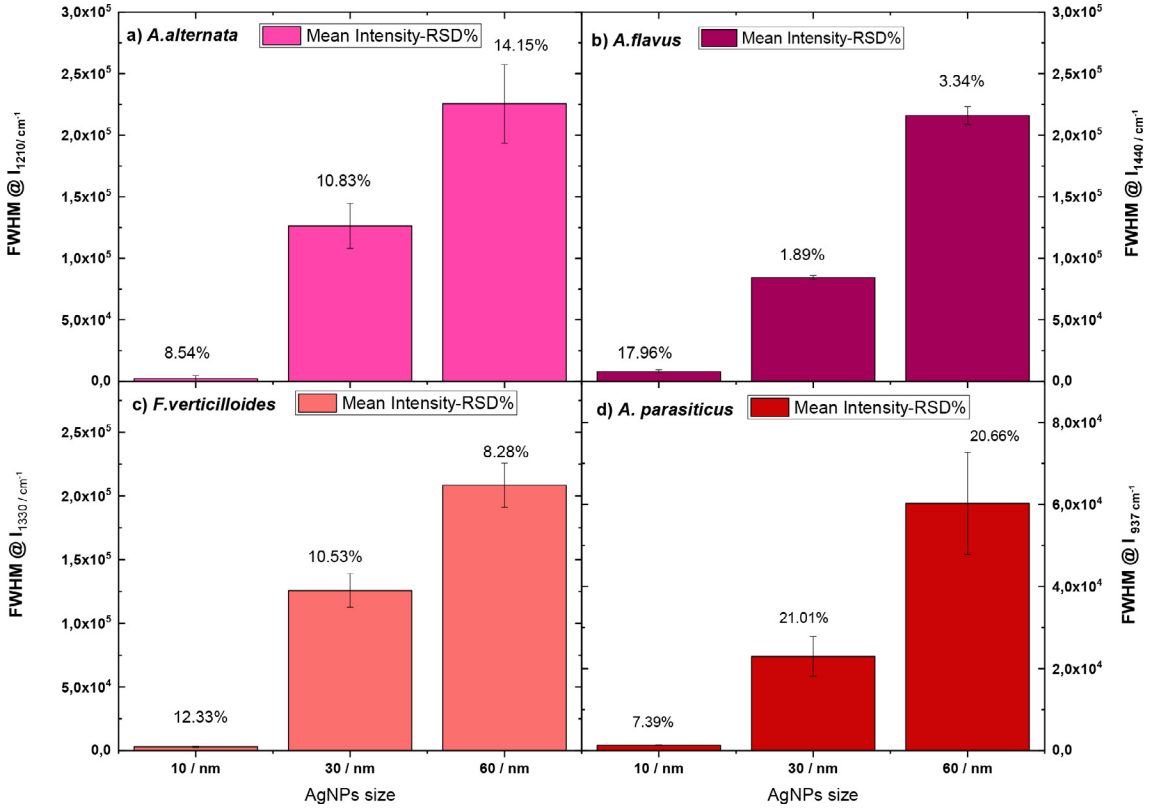

Fig. 3. The effect of AgNP size on the reproducibility at the selected band intensity in the SERS spectra of: a) *A.alternata*, b) *A. flavus*, c) *F. verticilloides*, d) *A. parasiticus*.

1700 cm^{-1}. However, 60 nm AgNPs had nearly twice the influence of 30 nm AgNPs on the SERS spectra of each fungus strain. There are no Raman signals in the NR spectra of each fungal strain without AgNPs as a control, save for a weak band intensity of approximately 1400 cm^{-1}, which could be due to background fluorescence, other researchers have reported same observations [40]. The SERS spectra of the four fungus strains using 10 nm AgNPs show very low SERS intensity in the 550–1100 cm^{-1} range, with only a weak broad peak about 1400 cm^{-1}, which is comparable to the NR spectra profile.

The SERS spectra of *A. alternata* using 60 nm AgNPs (Fig. 2a) shows strong peaks intensity at 1131, 1210, 1334, 1440, and 1575 cm^{-1} which almost doble the peak intensity using 30 nm AgNPs, and the SERS activity of 10 nm AgNPs is very weak across the whole wavenumber range of 1100 to 1650 cm^{-1}. When using 10 nm AgNPs the SERS spectra of A. flavus (Fig. 2b) displays minor weak peak intensities in the 550–1200 cm^{-1} area that are scarcely discernible except for a weak broad peak about 1400 cm^{-1} similar to NR spectra profile. The SERS spectra of A. flavus obtained with 60 nm AgNPs are about twice as intense as those produced with 30 nm AgNPs. In the

wavenumber range of 1100 to 1650 cm^{-1}, the SERS intensity displays strong bands at 1186, 1300, 1321, 1440, and 1577 cm^{-1}.

With an increase in the size of AgNPs from 10 to 60 nm, the SERS spectra of *F. verticilloides* show very high SERS intensity activity (Fig. 2.c). The SERS intensity of *F. verticilloides* shows strong peaks at 1250, 1330, 1458, and 1575 cm^{-1} in the wavenumber range of 1100 to 1650 cm^{-1}. It's worth noting that the peak intensity of the 60 nm AgNPs SERS spectra is nearly double that of the 30 nm one, and the SERS and NR spectra signals are barely discernible, with the exception of a weak band intensity about 1400 cm^{-1}.

A. paraciticus appears to have the lowest SERS intensity, 60 nm AgNPs yield large enhancement up to 6.0×10^4 across the whole wavenumber range of 550 to 1700 cm^{-1} when compared to the SERS intensities other three fungal strains, which yield enhancements up to 2.4×10^5, for the same size of AgNPs. Furthermore, when utilizing 30 nm AgNPs, the SERS intensity of *A parasiticus* increases approximately half as much as when using 60 nm AgNPs, and when using 10 nm AgNPs, no SERS activity is detected. The SERS intensity of *A. parasiticus* shows strong peaks at 612, 845, 937, 1176, 1288, 1370, 1512, and 1555 cm^{-1}.

The impact of AgNPs size on SERS enhancement in the four fungal strains investigated can be described in three approaches, which can occur separately or simultaneously. The first is electromagnetic enhancement, which involves the excitation of surface plasmons on silver nanostructures; the second is chemical enhancement, which involves the formation of a charge-transfer complex between AgNPs and fungi cell biomolecules; and the third is the quadruple effect, which involves the presence of fungi biomolecules in the vecinity of AgNPs. [21,22,29]. When spherical AgNPs are used for SERS, they need to be in groups and from the so-called ¨hot spots¨, which have higher free energies and are better for interacting with fungal molecules to improve SERS significantly. This would also imply that the active substrate fungi strain-AgNPs with smaller intraparticle gaps between neighboring AgNPs improves the active surface and facilitates contact with as many as biomolecules as feasible. As a result, it relates to the sensitivity of the substrate's limit of detection, which could suggest increased adsorption of biomolecules from fungal cell components onto the AgNPs surface; similar behavior has also been found in the SERS spectrum of bacteria and many other biomolecules [21,22]. This also implies that decreasing the inter-particle gap size of AgNP spheres increases the SERS signal intensity. That is, active substrate fungi-AgNPs with a smaller inter-particle gap between nearby aggregates have a stronger SERS signal. Furthermore, this could be due to the fact that as the gap size reduces, the density of the electromagnetic field between AgNPs increases, resulting in a

higher SERS signal. [22]. The average diameter of AgNPs increased from 10 to 60 nm, and the SERS intensity increased as the interparticle gap size of the aggregates narrowed. Furthermore, according to the quadruple effect, biomolecules of fungi in the vicinity of AgNPs'tips and wedges show increased polarization, the biomolecules are then attracted to these locations of minimal potential energy, resulting in significant enhancements. In this scenario, as the biomolecules get closer to the AgNPs, the SERS intensity increases due to the stronger electric field.

4.2. SERS reproducibility of filamentous fungi

The reproducibility of the recorded SERS signals from fungi is a critical parameter for future analytical applications of this approach in the detection and identification of filamentous fungi. The SERS spectra of each fungal strain studied were used to demonstrate the reproducibility of SERS signals, with a concentration of roughly 10^5 cfu/mL and 10, 30, and 60 nm AgNPs, with the most prominent peak intensity chosen due to the highest enhancement at this band as follows: I^{-1}_{1210cm} for *A. alternata*), $I^{-1}_{1440\ cm}$ for *A. flavus*), $I^{-1}_{1330\ cm}$ for *F. Verticilloides*), and I^{-1}_{937} for *A. parasiticus*. Fig. 5S (SM) shows a total of 15 SERS spectra from each of the fungus investigated, taken from different places within the same active substrate and from three different AgNP sizes. The full width at half maximum (FWHM), mean intensity (M), standard deviation (SD), and relative standard deviation (RSD) for each strain were calculated using the specified band (RSD%) (Table 1S, SM). Fig. 3 shows that when the AgNPs size increased, the Raman intensity increased. For example, compared to the size of 30 nm (1.1×10^5) for each fungus strain, the size of 60 nm (2.3×10^5) provided higher SERS intensity and sensitivity of the selected peak. The SERS signal reproducibilities for each AgNPs size of each examined fungus strain at their chosen peak intensity (RSD %) ranges from: 8.5–14% (*A. alternata*) at 1250 cm^{-1}; 1.9–18% (*A. flavus*) at 1440 cm^{-1}, 8–12% (*F. verticilloides*) at 1330 cm^{-1}; and 7–21% (*A. parasiticus*) at 937 cm^{-1} (Fig. 3a–c). For SERS quantitative studies, less than 20% variance in SERS intensity between different locations of the active substrate is acceptable, according to Wang et al. [30]. Except for *A. parasiticus* (RSD = 20.6%), all fungal strains had RSDs of less than 20% for 60 nm AgNPs. The maximum SERS intensity was found for 60 nm AgNPs, which could be attributed to an increase in the AgNPs' ability to bind to fungal biomolecules. 60 nm was chosen as the

best size in the current investigation based on both the SERS enhancement and the reproducibility of the peak selected in the SERS spectra; this result was consistent with the previous studies [22,32].

4.3. Evaluation of the SERS spectra

To evaluate the SERS spectra of *A. alternata*, *A. flavus*, *F. verticilloides*, and *A. parasiticus*, the most suitable AgNPs size (60 nm) was chosen. Fig. 4 exhibits the average SERS spectra observed from the four fungi studied, in the shape of dried thin film active substrate cast onto CaF_2 glass slide, and are exhibited in the wavenumber ranging between 550 and 1700 cm^{-1}. Table 2 show the complete lists of identified SERS bands with tentative peak assignments. The functional groups of aminoacids, nucleic acids, lipids, and carbohydrates are dominant in the SERS spectra of the four filamentous fungi investigated. The observed bands were assigned with reference to literature values for some fungi strains, common biochemical fungi cell wall components, and reference databases. Each filamentous fungi spectrum has distinct spectral features over the region of 550 to 1700 cm^{-1}. Two spectral windows, one between 550 and 1000 cm^{-1} are characterized by weak band intensities, position, and peak sharpness. The second spectral

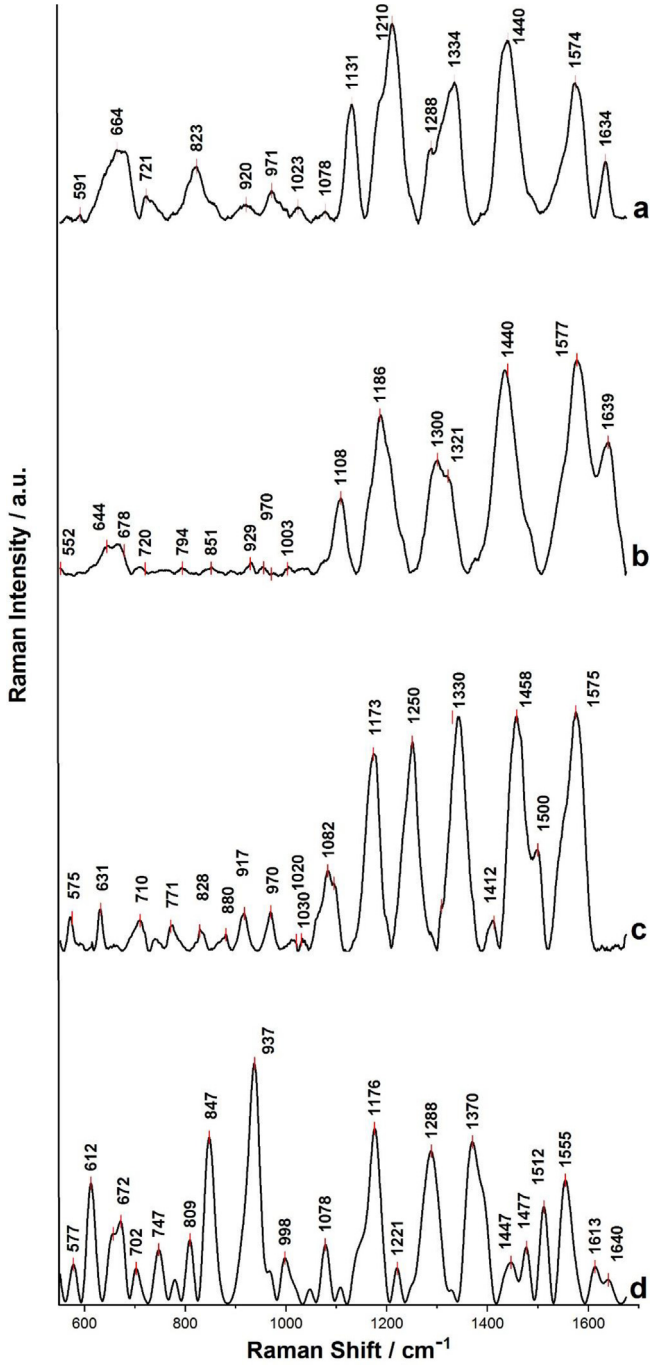

Fig. 4. The average SERS spectra of (a) *A.alternata*,(b) *A. Flavus*, (c) *F. verticilloides*, (d) *A.paraciticus* using AgNPs size with a size of 60 nm deposited onto CaF_2 cast as dried thin film. The following were the experimental conditions: 1% (500 mW), 785 nm excitation, 10 s exposure time. Each SERS spectrum was averaged from 15 tests recorded on random location on the same sample. All SERS spectra were baseline corrected, normalized and shifted vertically for improved visualization. Each SERS spectrum was averaged from 15 tests.

region between 1000 and 1700 cm^{-1} (fingerprint area) is characterized by strong broad and sharp intensities (Fig. 4a–c), with exception of the SERS of *A. paraciticus* (Fig. 4d), which shows considerable variety in shapes and low intensity bands..In the SERS spectra of *A. flavus*a weak band at 552 cm^{-1} was indentified, which was attributed to DNA/RNA bases such as thymine (T), cytosine (C) or guanine (G) with Phe twisting C-C. We observed weak low intensity bands at 575 cm^{-1} (*F.verticilloides*), 577 cm^{-1} (*A. paraciticus*) and 591 cm^{-1} (*A. alternata*), in the same spectral region, all of

Table 2
Positions in wavenumbers of the Raman Shift bands observed in the fungi spectra of *A. Alternata, F. Verticilloides, A. Flavus, A. Paraciticus.*

Tentative band assignment[†]	*A. Alternata*	*A. Flavus*	*F. Verticillioides*	*A. Parasiticus*	References[†]
DNA and RNA bases e.g. T/C, G; twist Phe, e.g.		552 (w)	575 (w)	577 (mw)	a, b, c
C—C twisitng mode of Phe	591 (mw)				c,d
C—C twisitng mode of Phe				612 (ms)	b,c
Aromatic bending, adenine, cytosine			631 (w)		a, e
Guanine	664 (ms)	644 (w)			a, c
Tyrosine		678 (w)		672 (m)	a, b
D-(+)-Trehalose				702 (w)	c, e
C—H rocking of > CH2, FDA, adenine, glycoside	721 (w)	720 (w)	710 (br)	747 (w)	a,b,c
v (O—P—O) RNA, Riboflavin, cytosine, uracil		794 (w)	771 (w)		a, b
υ(OPO)symmetric, υ(OPO)antisymmetric, phosphodiester	823 (ms)		828 (w)		c,d,e
e.g. lecithin,trilinolein, trilinolenin		851 (w)		847 (s)	a, f
v(CC), v(COC), carbohydrates			880 (m)		c, d
e.g. α or β-glucan, amilose, galactomannnan	920 (mw)	929 (w)	917 (m)	937 (vs)	c, e
v (C—C) proteins, C=C) def, v (C—N), e.g. chitin	971 (w)	970 (w)	970 (w)		f, g
Phe (skeletal), d (CH), e.g. protein assignment	1023 (mw)	1003 (w)	1020 (w)	998 (m)	b, e
def (C—H), C—N stretching, proteins, *e.g.* phenylalanine			1030 (w)		a, f
O—P—O (DNA), C—C or v C—O—C stretching,	1078 (mw)		1082 (vs)	1078 (m)	c, f
Carbohyddrates, e.g. 1,3-b glucan, chitin					
δ(C—H), Phe (protein assignment)	1131 (ms)	1108 (s)			b, d
δ(C—H), C—O ring, aromatic aminoacids in proteins		1186 (vs)	1173 (vs)	1176 (s)	a, c
e.g. tyrosine, hysitidine, proline					
Amide III , υantisymmetric PO2- str.	1210 (vs)		1250 (vs)	1221 (w)	a, b
Amide III (random), C, *e.g.* L-proline, triptophan	1288 (sh)	1300 (ms)		1288 (s)	b, g
Adenine, guanine, CH deformation	1334 (s)	1321 (sh)	1330 (vs)		b, e

(Table 2. (*continued*)

Tentative band assignment[†]	*A. Alternata*	*A. Flavus*	*F. Verticillioides*	*A. Parasiticus*	References[†]
T,A,G (ring breathing modes of purines and pyrimides)			1370 (s)	a,b,g	
CH2 bending, *e.g.* galactomannan					b, e
υ CH2, υ s CH3, e.g.lipids, trinolein, trilinolein	1440 (vs)	1440 (vs)	1412 (w)		c, f
Nucleic acid modes, CH2 def, CH3 def, eg. L-phe			1458 (vs)	1447 (sh)	d, g
CH2 def, e.g. L-proline				1477 (w)	a, b
Aminde II, C=C stretching in benzenoid ring, carotenoids			1500 (sh)	1512 (ms)	c, d
C=C bending mode of phenylalanine, *e.g.* hisitidine	1574 (s)	1577 (vs)	1575 (vs)	1555 (ms)	f, g
				1613 (w)	a, d
Amide I, C=O, plane N—H bending and C—N stretching	1634 (ms)	1639 (sh)	1638 (vw)	1640 (w)	a, g

Abreviations: (w), weak; (m), medium; (s), strong, (mw), medium weak; (ms) medium strong; (vs), very strong (vs); (sh), shoulder
[†] All the assignments are from references: (a) [31]; (b) [36]; (c) [37]; (d) [38]; (e) [33]; (f) [39]; (g) [35].
[†] υ, stretching; δ, bending; ρ, rocking; def, deformation; as, asymmetric; s,symmetric; C, cytosine; A,adenine; G,guanine; Phe, phenylalanine; Tyr, tyrosine.

which are associated with nucleic acids. The broad band at *ca.* 664 cm^{-1} in the SERS spectra of *A. alternata* (Fig. 4a) could be assigned to the ring breathing nucleic acids such as guanine, which also appears to have slightly shifted to a broad band between 644 cm^{-1} and 678 cm^{-1} in (*A. flavus*), which is assigned to the ring breathing of tyrosine. Another broad band at *ca.* 672 cm^{-1} (*A . paraciticus*) and moderately shifted to 631 cm^{-1} (*F. verticilloides*) is probably ascribed to cytosine. The following low intense band at 721 cm^{-1} (*A. alternata*) is assigned to FAD, riboflavin. This band fluctuates in intensity and shift to a low intensity band at 720 cm^{-1} (*A. flavus*), a broad band at 710 cm^{-1} (*F.verticilloides*), and two small bands at 747 cm^{-1} and 702 cm^{-1} in the SERS spectrum of *A. parasiticus*. Flavins are essential coenzymes that are found on the inside of bacterial and fungal cell walls and play a role in their formation. FDA and RF have been found to be effective AgNPs aggregates nucleation centers in or out the cell wall, ensuring their proximity to the AgNPs active site or hot spot [14]. Furthermore, the next weak band at 794 cm^{-1} in the SERS spectrum of *A. flavus*, drops and changes to 771 cm^{-1} in *F. verticilloides*, these bands can be assignable to cytosine and uracil. The broad band at 823 cm^{-1} (*A. Alternata*) can be ascribed to unsaturated O—P—O stretching, which can be symmetric or asymmetric such as phosphodiester. This band however is weakening in intensity and shifts to 828 cm^{-1} (*F. verticilloides*), 851 cm^{-1} (*A.flavus*) and 847 cm^{-1} (*A.paraciticus*). The Raman spectra of bases found in RNA *e.g.* thymine [31]. In addition, a weak band at *ca.* 880 cm^{-1} (*F. verticilloides*) can be seen in the Raman spectra of 1, 3-β-glucan. The prominent sharp intense band centered at 937 cm^{-1} in the spectral section of *A.prarsiticus* (Fig. 4d) is attributed to carbohydrates such as α or β-glucans, which are typical components comprising the fungal cell wall. This band (937 cm^{-1}) drops in intensity from 917 cm^{-1} (*F.verticiloides*) to 920 cm^{-1} (*A.alternata*) and 929 cm^{-1} (*A.flavus*). The following weak band at 971 cm^{-1} in the SERS of *A. alternata* can be assignable to C=C deformation of carbohydrates with some C—N stretching. In the SERS spectra of *F. verticilloides* this band increases slightly in intensity and shifts to 970 cm^{-1}, but in *A.flavus*, it decreases significantly in intensity; this variability suggests the possibility of overlapping peak in this region with a complex shape and low intensities bands. However, in the *A.parasiticus* sample, this shifts to a medium peak intensity of 998 cm^{-1}, which can be seen in the Raman spectrum of aminoacids such as tryptophan. We found progressive increases in band intensities from very low to extremely high in the spectral region between 1000 and 1700 cm^{-1} (fingerprint area). In the case of *A. flavus* we observed the very weak band at 1003 cm^{-1} assignable to C—C skeletal of phenylalanine. Besides, from the weak intensity band observed at 1023 cm^{-1} (*A. alternata*) and, two very weak peaks in *F.verticilloides* at 1020 and 1030 cm^{-1} that can be attributed to aminoacids or proteins (Fig. 4a–c, Table 2). This could be owing to a mismatch between the relative concentration of aminoacids found in the cell wall of different fungal strains and the SERS spectra, which have narrow band positions and low intensities. Moreover, the complex symmetrical mode of PO_2^- is composed of DNA and C—C, C—O—C, stretching, with a low intensity band at 1078 cm^{-1} in *A. alternata*, same value at mid intensity in *A. Parasiticus*, and a higher intensity band at 1082 cm^{-1} in *F. verticilloides*. These bands were found in the Raman spectrum of carbohydrate including 1, 3-β-glucan and chitin, both of which are common components of fungal spores. Chitin makes about 10–20% of the cell wall in *Aspergillus* strains [41,42]. The chitin material appears to be a fibrillar layer adjacent

to the plasma membrane, and is assumed to play a primarily structural role in the basal layer of the cell wall [32]. Similarly, at 1176 cm^{-1} (*A. parasiticus*), a broad and sharp band was seen, possibly due to C—O ring of aromatics aminoacids in proteins, such as tyrosyne. Two strong bands were also found in two fungi strains in the same spectral range, the first sharp at 1173 cm^{-1} (*F.verticilloides*) and the other broad at 1186 cm^{-1} (*A.flavus*). The adsorption behavior on AgNPs may be influenced by the relative abundance of protein component within their own structural morphological features. The *A. Alternata* SERS spectrum revealed a strong intense band at 1210 cm^{-1} (Fig. 4a), which was attributed to amide III asymmetric stretching of PO_2^-, probably from one phenylalanine or tyrosine. In *F. verticilloides*, this band (1210 cm^{-1}) shifts to a strong band at 1250 cm^{-1}, whereas in *A. parasiticus* it becomes less intense and shifts to 1221 cm^{-1}. The strong signal in the SERS spectra of *A. flavus* appears at 1440 cm^{-1} (Fig. 4b), at the same wavenumber, another peak this peak was also identified in the SERS spectra of *A. flavus* These signals have been found in the Raman spectra various fatty acids, such as trilinolenin, into the chemical composition of spores, which consist with the spore's fundamental biological function as an energy reserve for dispersal and reproduction [33,41]. Because of the relative abundance of each component present in each strains, a spectral relationship like this might exist in the SERS spectra of *F. verticilloides*, this band is declining and appears to have shifted to an extremely weak peak at 1412 cm^{-1}. The following band at 1131 cm^{-1} (*A.Alternata*) is most likely to δ(C—H) phenylalanine, and a medium strong broad band at 1108 cm^{-1} (*A.flavus*), which can be attributed to proteins. The strong band at 1330 cm^{-1} in the SERS spectra of *F. verticilloides* (Fig. 4c) can be assigned to CH bending with relative purine (adenine, guanine), and the peak at 1334 cm^{-1} (*A.Alternata*) includes a weak shoulder peak at 1288 cm^{-1}, both assigned to amide III.,. As described by Premasiri et al. [34], those signals are associated with degradation of nucleic acids and nucleotides due to cell starvation, which results in the release of adenine and guanine outside the cells. In addition, one strong band at 1288 cm^{-1} in the SERS spectrum of *A. paraciticus* can be attributed to amino acids. We found a broad band at 1300 cm^{-1}, with a shoulder peak at 1321 cm^{-1}, in the SERS spectra of *A. flavus*, which can also be assigned to amino acids such as L-proline and triptophan. Assigning the Raman band to specific groups is difficult due to the amide III vibrational mode'sensitivity and extremely complicated properties such as interaction with other vibrational bands. The strongwide band at 1458 cm^{-1} and its shoulder at 1500 cm^{-1} (*F.verticilloides*) can be assigned to amide II and possibly nucleic acids. The relatively high concentration of nucleic acids (purines) could be released from cells broken during the sample preparation, or some of the nanoparticles may have penetrated the cell wall and produced SERS signal from the purines inside the cell [35]. The broad band (1458 cm^{-1}) in the SERS spectra of *A. parasiticus*, appears to have dropped in intensity and shifted to a broad band 1477 cm^{-1}, which includes a shoulder peak probably attributable to L-phenylalanine and L-proline, respectively. Moreover, two bands, one sharp and low intensity at 1512 and the other broad and medium intensity at 1555 cm^{-1} in the SERS spectrum of *A. parasiticus*, were ascribed to amide II. The amide group involves primarily C=O stretching, in-plane modes of N—H bending, and υ (C—C) vibrational modes. The C=C bending of phenylalanine can be attributed to the strong band at 1574 cm^{-1} (*A. alternata*), which can also be observed in the SERS spectra of *A. flavus* at 1577 cm^{-1} and *F. verticilloides* at 1575 cm^{-1}, with slightly shifted to very intense bands. Furthermore, the weak band at 1634 cm^{-1} (*A. alternata*), could be ascribed to amide I. In the SERS spectra of A.*flavus*, a broad intense band at 1577 cm^{-1} with strong shoulder peak at 1639 cm^{-1}, in the same spectral range, we observed two low intense bands at ca. 1640 cm^{-1} and 1613 cm^{-1} in *A. parasiticus*, but none in *F. verticilloides*. The observed wavenumber range 1630–1695 cm^{-1} has been associated to the dominant secondary structure and the presence of β- plated sheet configuration in these strains [40]. Thus, these bands could be ascribed to C=O stretching coupled with the in plane N—H bending and C—N stretching bands.

A multivariate statistical analysis was also applied to better understand the discriminating between the four filamentous fungi studied, which is explored in more detail in the next section.

4.4. Statistical analysis of classification

Principal component analysis (PCA) in the spectrum range 1000–1700 was performed on all of the fungus studied, using AgNPs with a diameter of 60 nm: *A.alternata, A.flavus, F. verticilloides, and A.paraciticus*, and all of them have been connected to biodeterioration and biodegradation of cultural heritage objects. The three main components (PCs) (PC-1, PC-2, and PC-3) were found to be the most diagnostically significant, accounting for 56 %, 25%, and 18 % of the variation in the data set, respectively (Fig. 5a). The differences between the four fungi strains were examined base on their bands produced by the corresponding spectra in the previous section 3.3, and are clearly exhibited by loading plots in n Fig. 5b. The loading supplies information about the variables (spectrum wavenumbers) that are critical for group separation. The PC-1 loading plot indicated the most relevant diagnostic criteria in the analyzed data set, with high loading values indicating the most important variables for diagnostic purposes. Unlike the SERS spectrum, the loading spectrum has positive and negative bands, and the frequencies correspond to some of the significant fluctuation in the molecular composition of each fungi examined Fig. 6S (SM).

The most significant differences between the the four fungi were found to be associated with the main bands on the possitive side at *ca.* 1108, 1186, 1330 and 1440 cm^{-1} and the bands on the negative side at *ca.* 1131, 1250, 1334, and 1512 cm^{-1}, the band at 937 cm^{-1} correspeonding to *A. parasiticus* was not in the selected wavenumber of the spectrum. These vibrational modes corresponding particularly to cell wall composition of fungi such as aminoacids, nucleic acids, nucleotides, polysacharides and lipids, according to the SERS spectra analysis and loading plots from PC-1 (Fig. 4 and Table 2).

These macromolecules that come into direct contact with the AgNPs hot spots, where the scattering is enhanced [40]. Thus, the PCA analysis resolved for these four fungi in the fingerprint SERS spectral region (1000–1700 cm^{-1}) accounted for about 99% of the data variation (Fig. 5a–b). The above results indicate that the SERS spectra using AgNPs of 60 nm in combination with PCA had a high potential for identifying and detecting between four separated clusters corresponding to the *A.alternata, A.flavus, F. verticilloides and A.paraciticus* fungi strains, all of which are linked to biodeterioration and biodegradation cultural heritage materials.

5. Conclusions

AgNPs were synthesized by wet-chemical reduction, and SAXS was utilized to monitor and evaluate their shape and size to explore how the size of AgNPs impact the SERS performance of four filamentous fungi linked to biodeterioration and biodegradation of cultural heritage materials. With exception of *A. parasiticus*, which only achieved 6.0×10^4, the SERS spectrum increases in band intensities as AgNPs size increases from 10 to 60 nm, with the SERS enhancement up to 2.4×10^5 in comparison to NR, particularly in the 1000–1700 cm^{-1} spectral region (fingerprint area). In the recorded SERS spectra of each fungus studied, the RSD repro-

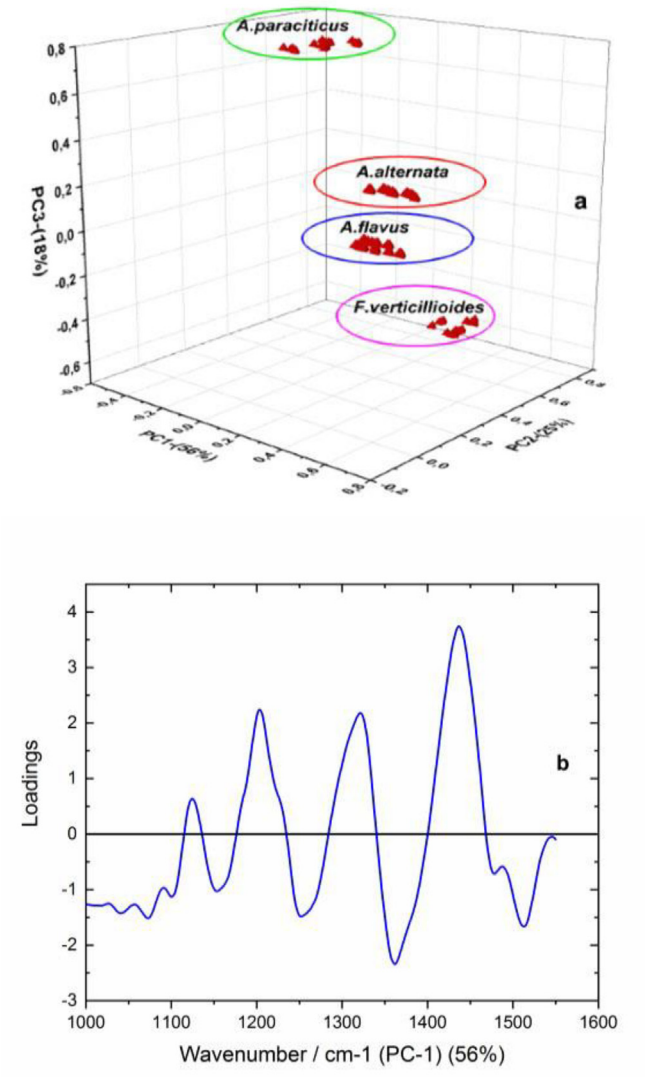

Fig. 5. Three PCs (PC-1, PC-2, and PC-3) a) scores plot 3D-PCA for the SERS spectra of four fungi investigated in the region (1000–1700 cm^{-1}b) Loding plot for the PC-1 showing the most significant bands in the spectral window.

ducibility of the selected peak intensities was less than 20%. As a consequence, 60 nm was considered as the most suitable size based on both SERS enhancement and reproducibility. The fingerprint area in the SERS spectra of each fungal strain using 60 nm AgNPs was investigated in detail, for example, the prominent band at 1440 cm^{-1} in the SERS spectra of *A.alternata* and *A.flavus*; 1412 cm^{-1}*F.verticilloides*, and 1447 cm^{-1} suggesting the presence of fatty acids from fungal spores, whose fundamental biological role is energy reserve for survival. PCA scores resolved by PC-1, PC-2, and PC-3 values accounted for roughly 99 percent of total variation in the fingerprint spectral region, confirming the clustering into four different clusters. The SERS approach, which employs 60 nm AgNPs in conjunction with PCA, offers a lot of potential for detecting and identifying different filamentous fungal strains.The SERS approach, which employs 60 nm AgNPs in conjunction with PCA, offers a lot of potential for detecting and identifying different filamentous fungal strains.

Declaration of Competing Interest

The authors declare the following financial interests/personal relationships which may be considered as potential competing interests: [Javier Christian Ramirez Perez reports was provided by University of Sao Paulo, Brazil. Javier Christian Ramirez Perez reports a relationship with Kent State University that includes: non-financial support. We declare no conflict of interest with any institution].

Acknowledgements

We gratefully acknowledge the support of Prof Dr. Fabio Rodrigues and MSc. Evandro P. da Silva, Brazilian Research Unity in Astrobiology - NAP/Astrobio at USPIQ- (University of Sao Paulo) for allowing spectral analysis and valuable assistance, Prof. Dr. Beneito Correa, Laboratory of Mycology at Institute of Biosciences at USP for encouragement, Dr. Paulo Garcia Brazilian Center for Research in Energy and Materials (CNPEM)/ Brazilian Synchrotron Light Laboratory (LNLS) for helpful assistance.

Appendix A. Supplementary material

Supplementary data to this article can be found online at https://doi.org/10.1016/j.saa.2022.120980.

References

[1] C. Santos, M. Fraga, Z. Kozakiewicz, N. Lima, Fourier transform infrared as powerful technique for identification and characterization of filamentous fungi and yeast, Res. Microbiol. 161 (2010) (2010) 168–175.
[2] L. Domingues, N. Lima, J.A. Texeira, Aspeergillus Níger b-galactosidase production by yeast in continuous high cell density reactor, Process Biochem 40 (2005) (2005) 1151–1154.
[3] V. Eukhimocitch, V. Pavlov, M. Talyshinsky, Y. Souprum, M. Huleihel, FTIR microspcopy as a method for identification of bacterial and fungal infections, J. Pharm. Biomed. Anal. 37 (2005) 1105–1108.
[4] A. Lecellier, J. Mounier, V. Gaydou, L. Castrec, G. Barbier, W. Ablain, A. Manfait, D. Toubas, G.D. Sockalingum, Differentiation and identification of filamentous fingi by high-throughput FITR spectroscopic analysis of mycelia, Int. J. Food Microbiol. 168–169 (2014) 32–41.
[5] H. Taylor, S.M. Latham, M.E. Woolhouse, Risk factors for human disease emergence, Philos. Trans. R.Soc. London, Ser.B. 356 (2001) 983–989.
[6] K. Kavkler, Z. Smit, E.D. Jezersek, A. Demsar, Investigation of biodeteriorated historical textiles by conventional and synchrotron radiation FITR spectroscopy, Polym. Degrad. Stab. 96 (2011) 1081–1086.
[7] K. Sterflinger, Fungi: their role in deterioration of cultural heritage, Fungal Biol. Rev. 24 (2010) 47–55.
[8] L. Sabatini, M. Sisti, R, Campana, Evaluation of fungal community involved in the biodeterioration process of wooden artworks and canvases in Montefeltro area (Marche, Italy), Microbiol. Res. 207 (2018) 203–210.
[9] J.C. Ramirez-Perez, Biotecnologia aplicada a la conservación de objetos de patrimonio cultural mediante el uso de radiación gamma. Revista de la Asociacion Latinoamericana de Tecnología de la Irradiación (ALATI en Contacto), Num. 3 (2019), 3.pdf (accessed 02.07.19 http://www.alati.la/encontacto/descargas/ALATI-en-contacto-Num.
[10] Ramirez-Perez J.C. Aerobic Biodegradation Kinetics of Solid Organic Wastes, LAMBERT ACADEMIC PUBLISHING (Eds.) Saabrücken, Germany, 2013
[11] J. Vukojevic, M. Ljaljevic-Grbic, Moulds on paintings, Zbornic. Matice Srp.za Prir. Nauke. (109) (2005) 175–179, https://doi.org/10.2298/ZMSPN0519175V.
[12] O. Ciferri, Microbial degradation of paintings, Appl. Environ. Microb. 65 (3) (1999) 879–885.
[13] K. Kavkler, N. Gunde-Cimerman, P. Zalar, A. Demsar, Fungal contamination of textile objects preserved in Slovene museums and religious institutions, Int. Biodeterior. Biodegrad. 97 (2015) 51–59.
[14] Abdel-Kareem O. Fungal deterioration of historical textiles and approaches for their control in Egipt (2010). online at http://www.morana-rtd.com/e-preservationscience/2010/Abdel-Kareem-15-01-2010.pdf (accessed 07.06.10).
[15] Who, Guidelines for Indoor Air Quality Dampness and Moulds, World Health Organization, Copenhagen, Denmark, 2009.
[16] G. Nja, P. Bouvrette, S. Hrapvic, J.H. Luong, Raman-based detection of bacteria using silver nanoparticles conjugated with antibodies, The Royal Society of Chemistry, the Analyst. 132 (2007) 679–686.
[17] P. Rabinow, Making PCR: A story of biotechnology, University of Chicago Press, Chicago, 1996.
[18] S. Stöckel, J. Kirchhoff, U. Neugebauer, P. Rtösh, J. Popp, The application of Raman spectroscopy for detection and identification of microorganisms, J. Raman Spectrosc. 47 (2016) 89–109.
[19] S. Efrima, L. Zeiri, Understanding SERS of Bacteria, J. Raman Spectros. 40 (3) (2009) 277–288.
[20] M. Karaman, M.M. Yazici, F. Sahin, M. Culha, Convective assembly of bacateria for surface-enhanced Raman scattering, Langmuir 24 (3) (2008) 849–901.

[21] J. Zhang, X. Li, X. Sun, Y. Li, Surface enhanced Raman scattering effects of silver colloids of different shapes, J. Phys. Chem. B 109 (2005) 12544–12548.
[22] Pan T-Pan, Sun D-Wen, Pu, H.,Wei, Q., Xiao W., Wang Q-Jun. Detection of A. alternata from pear juice using surface-enhanced Raman spectroscopy based silver nanodots array. J.of Food Engineering 215 (2017) 147-155
[23] H. Wang, X. Qiao, J. Chen, S. Ding, Preparation of silver nanoparticles by chemical reduction method, Coll. Surf. A: Physicochem. Eng. Aspects. 256 (2-3) (2005) 111–115.
[24] Banerjee, S., Loza, K., Meyer-Zaika, W., Prymak, O., Epple, M. Structural Evolution of Silver Nanoparticles during Wet-Chemical Synthesis,Chemistry of Materials.26 (2) (2014) 951-957xChen, LY., Mungroo, N., Daikura, L., Neethirajan, S. Label-free NIR-SERS discrimination and detection of foodborne bacteria by in situ synthesis of Ag colloids. J.Nanobiotechnology. 13 (2015) 45-53.
[25] P.R.A.F. Garcia, O. Prymak, V. Grasmik, K. Pappert, W. Wlysses, L. Otubo, M. Epple, C.L.P. Oliveira, An in situ SAXS investigation of the formation of silver nanoparticles and bimetallic silver–gold nanoparticles in controlled wet-chemical reduction synthesis, Nanoscale Adv. 2 (1) (2020) 225–238.
[26] A.T. Fazio, M.M. Lopez, M. Temperini, D.L. deFaria, Surface enhanced Raman spectroscopy and cultural heritage biodeterioration: Fungi identification in earthen architecture from Paraiba valley (São Paulo, Brazil), Vib. Spectrosc. 97 (2018) 129–134.
[27] H.H. Wang, C.C. Liu, S.B. Wu, N.W. Liu, C.Y. Peng, Highly Raman enhancing substrates based on silver nanoparticle arrays with tumable sub-10 nm gaps, Adv. Mater. 18 (4) (2006) 491–495.
[28] Lindner, P. a. Z.Th. 1991, Neutron, X-ray and light scattering: introduction to an investigative tool for colloidal and polymeric systems.
[29] A. Sabur, M. Havel, Y. Gogotsi, SERS intensity optimization by controlling the size and shape of faceted gold nanoparticles, J. Raman Spectrosc. 39 (2008) 61–67.
[30] E.C. Le Ru, E. Blackie, M. Meyer, P.G. Etchegoin, Surface enhanced Raman scattering enhancement factors: A comprehensive study, J. Phys. Chem. 111 (2007) 13794–13803.
[31] N.E. Dina, A. Colnita, N. Leopold, C. Haisch, Rapid single-cell detection and identification of bacteria by using surfacce-enhanced Raman spectroscopy, Procidia, Technology. 27 (2017) 203–207.
[32] F. Matsumoto, M. Ishikawa, K. Nishio, H. Masuda, Optical properties of long range-ordered high-density gold nanodot arrays prepared using anodic porous alumina, Chem. Lett. 34 (4) (2005) 508–509.
[33] J. De Gelder, K. De Gussem, P. Vandenabeele, L. Moens, Reference database of Raman spectra of biological molecules, J. of Raman Spectroscopy. 38 (2007) 1133–1147.
[34] K. Pietzak, S. Glinska, M. Gapinska, T. Ruman, A. Nowak, E. Aydin, B. Gutarowska, Silver nanoparticles: a mechanism of action of moulds, Metallomics Royal Society of Chemistry. 13 (2006) (2016) 7–11.
[35] K. De Gussem, P. Vnadenabeele, A. Verbeken, L. Moens, Raman Spectroscopic study of Lactarius spores (Russulales, Fungi), J. Spectrochimica Acta Part A. 61 (2005) 2896–2908.
[36] W.R. Premasiri, D.T. Moir, L.D. Ziegler, Vibrational fingerprint of bacterial pathogens by Surfacce enhanced Raman scattering (SERS), Int. Soc. Opt. Eng. 5795 (2005) 19–29.
[37] J. C. Ramirez-Perez, T. Alves dos Reis, and M. Rizzutto, Identifying and detecting Entomopathogenic fungi using Surface-enhanced Raman spectroscopy, Brazilian Journal of Animal and Environmental Research, 4, 4832-4850. https://doi.org/10.34188/bjaerv4n4-002
[38] Huang W. E., Li, M., Jarvis R.M., Giidacare, R., and Banwart S, Shining light on the microbial world: the application of Raman microspectroscopy, Advances in Applied Microbiology, , Elsevier Inc., Vol 70 (Chapter 5) London 2010.
[39] K. Malequin, C. Kirschner, L.P. Choo-Smith, N. van den Braak, H. Endtz, D. Naumann, G.J. Puppels, Identification of medically relevant microorganisms by vibrational spectroscopy, J. of Microbiological methods. 51 (2002) 255–271.
[40] M. Prusinkiewicz, D.JJ. Farazkhorasani, J. Wang, K. Gough, S. Kaminsky, Prof-of-principle for SERS imaging of *Aspergillus nidulans* hyphae ising in vivo synthesis of gold nanoparticles, Analyst. 137 (2012) 4934–4942.
[41] K. De Gussem, P. Vandenabeele, A. Verbeken, L. Moens, Chemotaxonomical identification of spores of macrofungi: possibilities of Raman spectroscopy, Anal Bioanal. Chem. 387 (8) (2007) 2823–2832.
[42] Z. Luo, L. Chen, C. Liang, Q. Wei, Y. Chen, J. Wang, Porous carbon fims decorated with silver nanoparticles as sensitive SERS substrate, and their application to virus indentification, Microchim Acta. 184 (2017) 3505–3511.